

# Search for dark matter towards the Galactic Centre with 11 years of ANTARES data

A. Albert<sup>1,2</sup>, M. André<sup>3</sup>, M. Anghinolfi<sup>4</sup>, G. Anton<sup>5</sup>, M. Ardid<sup>6</sup>, J.-J. Aubert<sup>7</sup>, J. Aublin<sup>8</sup>, B. Baret<sup>8</sup>, S. Basa<sup>9</sup>, B. Belhorma<sup>10</sup>, V. Bertin<sup>7</sup>, S. Biagi<sup>11</sup>, M. Bissinger<sup>5</sup>, J. Boumaaza<sup>12</sup>, M. Bouta<sup>13</sup>, M.C. Bouwhuis<sup>14</sup>, H. Brânzaş<sup>15</sup>, R. Bruijn<sup>14,16</sup>, J. Brunner<sup>7</sup>, J. Busto<sup>7</sup>, A. Capone<sup>17,18</sup>, L. Caramete<sup>15</sup>, J. Carr<sup>7</sup>, S. Celli<sup>17,18,19</sup>, M. Chabab<sup>20</sup>, T. N. Chau<sup>8</sup>, R. Cherkaoui El Moursli<sup>12</sup>, T. Chiarusi<sup>21</sup>, M. Circella<sup>22</sup>, A. Coleiro<sup>8</sup>, M. Colomer-Molla<sup>8,23</sup>, R. Coniglione<sup>11</sup>, P. Coyle<sup>7</sup>, A. Creusot<sup>8</sup>, A. F. Díaz<sup>24</sup>, G. de Wasseige<sup>8</sup>, A. Deschamps<sup>25</sup>, C. Distefano<sup>11</sup>, I. Di Palma<sup>17,18</sup>, A. Domi<sup>4,26</sup>, C. Donzaud<sup>8,27</sup>, D. Dornic<sup>7</sup>, D. Drouhin<sup>1,2</sup>, T. Eberl<sup>5</sup>, N. El Khayati<sup>12</sup>, A. Enzenhöfer<sup>5,7</sup>, A. Ettahiri<sup>12</sup>, P. Fermani<sup>17,18</sup>, G. Ferrara<sup>11</sup>, F. Filippini<sup>21,28</sup>, L. Fusco<sup>8,21</sup>, P. Gay<sup>8,29</sup>, H. Glotin<sup>30</sup>, R. Gozzini<sup>23</sup>, R. Gracia Ruiz<sup>1</sup>, K. Graf<sup>5</sup>, C. Guidi<sup>4,26</sup>, S. Hallmann<sup>5</sup>, H. van Haren<sup>31</sup>, A.J. Heijboer<sup>14</sup>, Y. Hello<sup>25</sup>, J.J. Hernández-Rey<sup>23</sup>, J. Höfl<sup>5</sup>, J. Hofestädt<sup>5</sup>, F. Huang<sup>1</sup>, G. Illuminati<sup>23</sup>, C. W. James<sup>32</sup>, M. de Jong<sup>14,33</sup>, P. de Jong<sup>14</sup>, M. Jongen<sup>14</sup>, M. Kadler<sup>34</sup>, O. Kalekin<sup>5</sup>, U. Katz<sup>5</sup>, N.R. Khan-Chowdhury<sup>23</sup>, A. Kouchner<sup>8,35</sup>, I. Kreykenbohm<sup>36</sup>, V. Kulikovskiy<sup>4,37</sup>, R. Lahmann<sup>5</sup>, R. Le Breton<sup>8</sup>, D. Lefèvre<sup>38</sup>, E. Leonora<sup>39</sup>, G. Levi<sup>21,28</sup>, M. Lincetto<sup>7</sup>, D. Lopez-Coto<sup>40</sup>, S. Loucatos<sup>41,8</sup>, G. Maggi<sup>7</sup>, J. Manczak<sup>23</sup>, M. Marcelin<sup>9</sup>, A. Margiotta<sup>21,28</sup>, A. Marinelli<sup>42,43</sup>, J.A. Martínez-Mora<sup>6</sup>, R. Mele<sup>44,45</sup>, K. Melis<sup>14,16</sup>, P. Migliozzi<sup>44</sup>, M. Moser<sup>7</sup>, A. Moussa<sup>13</sup>, R. Muller<sup>14</sup>, L. Nauta<sup>14</sup>, S. Navas<sup>40</sup>, E. Nezri<sup>9</sup>, C. Nielsen<sup>8</sup>, A. Nuñez-Castiñeyra<sup>7,9</sup>, B. O’Fearraigh<sup>14</sup>, M. Organokov<sup>1</sup>, G.E. Păvălaş<sup>15</sup>, C. Pellegrino<sup>21,28</sup>, M. Perrin-Terrin<sup>7</sup>, P. Piattelli<sup>11</sup>, C. Poirè<sup>6</sup>, V. Popa<sup>15</sup>, T. Pradier<sup>1</sup>, N. Randazzo<sup>39</sup>, S. Reck<sup>5</sup>, G. Riccobene<sup>11</sup>, A. Sánchez-Losa<sup>22</sup>, D. F. E. Samtleben<sup>14,33</sup>, M. Sanguineti<sup>4,26</sup>, P. Sapienza<sup>11</sup>, F. Schüssler<sup>41</sup>, M. Spurio<sup>21,28</sup>, Th. Stolarczyk<sup>41</sup>, B. Strandberg<sup>14</sup>, M. Taiuti<sup>4,26</sup>, Y. Tayalati<sup>12</sup>, T. Thakore<sup>23</sup>, S.J. Tingay<sup>32</sup>, A. Trovato<sup>11</sup>, B. Vallage<sup>41,8</sup>, V. Van Elewyck<sup>8,35</sup>, F. Versari<sup>21,28,8</sup>, S. Viola<sup>11</sup>, D. Vivolo<sup>44,45</sup>, J. Wilms<sup>36</sup>, D. Zaborov<sup>7</sup>, A. Zegarelli<sup>17,18</sup>, J.D. Zornoza<sup>23</sup>, and J. Zúñiga<sup>23</sup>

<sup>1</sup>Université de Strasbourg, CNRS, IPHC UMR 7178, F-67000 Strasbourg, France

<sup>2</sup>Université de Haute Alsace, F-68200 Mulhouse, France

<sup>3</sup>Technical University of Catalonia, Laboratory of Applied Bioacoustics, Rambla Exposició, 08800 Vilanova i la Geltrú, Barcelona, Spain

<sup>4</sup>INFN - Sezione di Genova, Via Dodecaneso 33, 16146 Genova, Italy

<sup>5</sup>Friedrich-Alexander-Universität Erlangen-Nürnberg, Erlangen Centre for Astroparticle Physics, Erwin-Rommel-Str. 1, 91058 Erlangen, Germany

<sup>6</sup>Institut d’Investigació per a la Gestió Integrada de les Zones Costaneres (IGIC) - Universitat Politècnica de València. C/ Paranimf 1, 46730 Gandia, Spain

- <sup>7</sup>Aix Marseille Univ, CNRS/IN2P3, CPPM, Marseille, France
- <sup>8</sup>Université de Paris, CNRS, Astroparticule et Cosmologie, F-75013 Paris, France
- <sup>9</sup>Aix Marseille Univ, CNRS, CNES, LAM, Marseille, France
- <sup>10</sup>National Center for Energy Sciences and Nuclear Techniques, B.P.1382, R. P.10001 Rabat, Morocco
- <sup>11</sup>INFN - Laboratori Nazionali del Sud (LNS), Via S. Sofia 62, 95123 Catania, Italy
- <sup>12</sup>University Mohammed V in Rabat, Faculty of Sciences, 4 av. Ibn Battouta, B.P. 1014, R.P. 10000 Rabat, Morocco
- <sup>13</sup>University Mohammed I, Laboratory of Physics of Matter and Radiations, B.P.717, Oujda 6000, Morocco
- <sup>14</sup>Nikhef, Science Park, Amsterdam, The Netherlands
- <sup>15</sup>Institute of Space Science, RO-077125 Bucharest, Măgurele, Romania
- <sup>16</sup>Universiteit van Amsterdam, Instituut voor Hoge-Energie Fysica, Science Park 105, 1098 XG Amsterdam, The Netherlands
- <sup>17</sup>INFN - Sezione di Roma, P.le Aldo Moro 2, 00185 Roma, Italy
- <sup>18</sup>Dipartimento di Fisica dell'Università La Sapienza, P.le Aldo Moro 2, 00185 Roma, Italy
- <sup>19</sup>Gran Sasso Science Institute, Viale Francesco Crispi 7, 00167 L'Aquila, Italy
- <sup>20</sup>LPHEA, Faculty of Science - Semlali, Cadi Ayyad University, P.O.B. 2390, Marrakech, Morocco.
- <sup>21</sup>INFN - Sezione di Bologna, Viale Berti-Pichat 6/2, 40127 Bologna, Italy
- <sup>22</sup>INFN - Sezione di Bari, Via E. Orabona 4, 70126 Bari, Italy
- <sup>23</sup>IFIC - Instituto de Física Corpuscular (CSIC - Universitat de València) c/ Catedrático José Beltrán, 2 E-46980 Paterna, Valencia, Spain
- <sup>24</sup>Department of Computer Architecture and Technology/CITIC, University of Granada, 18071 Granada, Spain
- <sup>25</sup>Géoazur, UCA, CNRS, IRD, Observatoire de la Côte d'Azur, Sophia Antipolis, France
- <sup>26</sup>Dipartimento di Fisica dell'Università, Via Dodecaneso 33, 16146 Genova, Italy
- <sup>27</sup>Université Paris-Sud, 91405 Orsay Cedex, France
- <sup>28</sup>Dipartimento di Fisica e Astronomia dell'Università, Viale Berti Pichat 6/2, 40127 Bologna, Italy
- <sup>29</sup>Laboratoire de Physique Corpusculaire, Clermont Université, Université Blaise Pascal, CNRS/IN2P3, BP 10448, F-63000 Clermont-Ferrand, France
- <sup>30</sup>LIS, UMR Université de Toulon, Aix Marseille Université, CNRS, 83041 Toulon, France
- <sup>31</sup>Royal Netherlands Institute for Sea Research (NIOZ) and Utrecht University, Landsdiep 4, 1797 SZ 't Horntje (Texel), the Netherlands
- <sup>32</sup>International Centre for Radio Astronomy Research - Curtin University, Bentley, WA 6102, Australia
- <sup>33</sup>Huygens-Kamerlingh Onnes Laboratorium, Universiteit Leiden, The Netherlands
- <sup>34</sup>Institut für Theoretische Physik und Astrophysik, Universität Würzburg, Emil-Fischer Str. 31, 97074 Würzburg, Germany
- <sup>35</sup>Institut Universitaire de France, 75005 Paris, France
- <sup>36</sup>Dr. Remeis-Sternwarte and ECAP, Friedrich-Alexander-Universität Erlangen-Nürnberg, Sternwartstr. 7, 96049 Bamberg, Germany
- <sup>37</sup>Moscow State University, Skobel'syn Institute of Nuclear Physics, Leninskie gory, 119991 Moscow, Russia
- <sup>38</sup>Mediterranean Institute of Oceanography (MIO), Aix-Marseille University, 13288, Marseille, Cedex 9, France; Université du Sud Toulon-Var, CNRS-INSU/IRD UM 110, 83957, La Garde Cedex, France
- <sup>39</sup>INFN - Sezione di Catania, Via S. Sofia 64, 95123 Catania, Italy
- <sup>40</sup>Dpto. de Física Teórica y del Cosmos & C.A.F.P.E., University of Granada, 18071 Granada, Spain
- <sup>41</sup>IRFU, CEA, Université Paris-Saclay, F-91191 Gif-sur-Yvette, France
- <sup>42</sup>INFN - Sezione di Pisa, Largo B. Pontecorvo 3, 56127 Pisa, Italy
- <sup>43</sup>Dipartimento di Fisica dell'Università, Largo B. Pontecorvo 3, 56127 Pisa, Italy
- <sup>44</sup>INFN - Sezione di Napoli, Via Cintia 80126 Napoli, Italy
- <sup>45</sup>Dipartimento di Fisica dell'Università Federico II di Napoli, Via Cintia 80126, Napoli, Italy

April 20, 2020

## Abstract

Neutrino detectors participate in the indirect search for the fundamental constituents of dark matter (DM) in form of weakly interacting massive particles (WIMPs). In WIMP scenarios, candidate DM particles can pair-annihilate into Standard Model products, yielding considerable fluxes of high-energy neutrinos. A detector like ANTARES, located in the Northern Hemisphere, is able to perform a complementary search looking towards the Galactic Centre, where a high density of dark matter is thought to accumulate. Both this directional information and the spectral features of annihilating DM pairs are entered into an unbinned likelihood method to scan the data set in search for DM-like signals in ANTARES data. Results obtained upon unblinding 3170 days of data reconstructed with updated methods are presented, which provides a larger, and more accurate, data set than a previously published result using 2101 days. A non-observation of dark matter is converted into limits on the velocity-averaged cross section for WIMP pair annihilation.

## 1 Introduction: dark matter signals at neutrino telescopes

The existence of cold, non-baryonic dark matter (DM), evidenced on macroscopic scale by astrophysical observations [1], encourages the searches for its possible particle constituents. Among those candidates, most WIMP scenarios accommodate the DM relic density reported by astrophysical measurements through a freeze-out mechanism. This could imply that typical WIMP interactions of the DM candidate, especially its annihilation cross section, lie near the electroweak scale; beyond that, other parameters like the candidate WIMP mass or the specific details of the DM model are left unbound. Under the hypothesis that a WIMP coincides with its antiparticle, indirect searches for WIMPs are possible by detecting a signature of WIMP annihilation into Standard Model particles. Such signals are therefore searched from the direction of massive astrophysical environments, where WIMPs can be gravitationally attracted. DM builds up in and around massive celestial bodies and gravitational accumulators, and is organized in *halos* and *clumps*. The distribution of dark matter with density  $\rho$  at a given sky location  $(r, \theta, \phi)$  is described through the  $J$ -factor

$$J = \int_{\Omega} d\Omega(\theta, \phi) \int_{\text{l.o.s.}} \rho^2(s(r, \theta, \phi)) ds, \quad (1)$$

with  $\Omega$  being the solid angle under which the source is observed, and  $s$  the radial coordinate integrated over the line of sight (l.o.s.) (see [2] for a detailed discussion). For neutrino telescopes, which have a very broad field of view, values as large as  $10^\circ - 30^\circ$  can be considered for the opening angle characterising the solid angle  $\Omega$ . Preferred locations where dark matter is predicted to accumulate are:

1. the Galactic Centre, having the largest  $J$ -factor;
2. massive, non-luminous galaxies like dwarf spheroidals;
3. the Sun or other nearby very massive celestial bodies.

DM messengers for indirect searches are neutrinos,  $\gamma$  rays or charged cosmic rays ( $e^+$ ,  $\bar{p}$ ), produced either as primary or as secondary products of a WIMP pair annihilation, through different channels. The Galactic Centre is not only a promising source for its large predicted DM density; it is also a target of complementary searches for neutrino detectors and  $\gamma$ -ray telescopes, due to the low source contamination that would give way to an unambiguous signal identification. Lastly, the Galactic Centre is in good visibility for neutrino telescopes located in the Northern Hemisphere (as will be clarified in Section 2), or for  $\gamma$ -ray telescopes installed in the Southern Hemisphere. The flux of neutrinos reaching the Earth from a WIMP pair annihilation can be expressed as a function of the thermally averaged cross section  $\langle\sigma v\rangle$  for WIMP pair annihilation, of the energy distribution of outgoing particles per WIMP pair collision  $dN/dE_\nu$ , and of the DM distribution represented by the  $J$ -factor:

$$\frac{d\Phi(E_\nu)}{dE_\nu} = \frac{1}{4\pi M_{\text{WIMP}}^2} \frac{\langle\sigma v\rangle}{2} \frac{dN(E_\nu)}{dE_\nu} J, \quad (2)$$

where the factor  $1/2$ , used in this analysis, holds for self-conjugate WIMPs, and is to be replaced by a factor  $1/4$  otherwise. Similarly, the term  $1/M_{\text{WIMP}}^2$  arises from the presence of two WIMPs in the process, keeping into account that both the mass and the volumetric density are expressed in energy units. Through the relation in Equation (2), a measurement of the integrated neutrino and antineutrino flux from the region of the Galactic Centre

$$\Phi_{\nu+\bar{\nu}} = \int dE_\nu \frac{d\Phi_\nu}{dE_\nu} + \int dE_{\bar{\nu}} \frac{d\Phi_{\bar{\nu}}}{dE_{\bar{\nu}}} \quad (3)$$

is converted into limits on the thermally averaged cross section  $\langle\sigma v\rangle$  for WIMP pair annihilation. A lower bound on this quantity of  $3 \cdot 10^{-26} \text{ cm}^3 \text{ s}^{-1}$  can be made based upon cosmology arguments [3].

## 1.1 Directional and morphological information

Indirect searches for dark matter are unavoidably subject to large uncertainties, mostly arising from the parameterisation of the unknown DM distribution. The spherically averaged DM density profile  $\rho$  contained in the  $J$ -factor (Equation (1)) is modelled according to different assumptions, leading to considerably different results. The main assumptions on  $\rho$  are based on cosmological N-body simulation results and/or dynamical constraints on the Milky Way or spiral galaxies. Even if baryonic physics (star formation and feedbacks) is not fully under control in hydrodynamics simulations, the baryons may steepen or even flatten the inner behaviour of the DM profile (see e.g. [4, 5, 6, 7]). Alternatively, dynamical studies of galaxies show a large diversity in rotation curves [8] and can suggest a cored DM profile [9, 10]. A popular and simple parameterisation of the DM density obtained in pure (without baryons) DM cosmological simulations is the Navarro-Frenk-White (NFW) profile [11]:

$$\rho_{\text{NFW}}(r) = \frac{\rho_0}{\frac{r}{r_s} \left(1 + \frac{r}{r_s}\right)^\gamma} \quad (4)$$

with  $\gamma = 2$ . The NFW profile is adopted in the present analysis with  $\rho_0 = 1.40 \cdot 10^7 \text{ M}_\odot/\text{kpc}^3$  and  $r_s = 16.1 \text{ kpc}$  [12]. For the sake of illustrating those DM density uncertainties, other two cases are considered: the profile from the recent study of McMillan [13] giving an internal power law  $r^{0.79 \pm 0.32}$ , and the Burkert profile [14] for which the inner density is constant.

## 1.2 Energy Information

The energy distribution of a neutral massive particle pair-annihilating into Standard Model products can be effectively described with a Monte Carlo generator such as PYTHIA or HERWIG [15, 16]. The PPC4 *cookbook* [17], used in this analysis, directly provides spectra for WIMP annihilations into Standard Model modes which are straightforward to adapt to any kind of indirect searches.

PPPC4 yields the energy distribution for an isotropic flux of Standard Model particles originated in the WIMP pair annihilation at the source. Several final states of the annihilation process, resulting in different decay modes ( $\tau^+\tau^-$ ,  $W^+W^-$ ,  $b\bar{b}$ ,  $\mu^+\mu^-$ ,  $\nu\bar{\nu}$ ) have been simulated, evaluating the spectrum of the resulting neutrino flux,  $dN_\nu/dE_\nu$ , for each WIMP mass. Each channel is considered with a 100% branching ratio (BR). Note that the matter density in the Galactic Centre is not enough to cause distortions or absorption effects in outcoming neutrino spectra.

Flavour oscillations occur between source and detection point. The three neutrino flavours are equally produced in WIMP pair annihilations, and the data set considered here only contains muon neutrinos recorded at the detector. The oscillations  $\nu_e, \nu_\tau$  into  $\nu_\mu$ , as well as the loss of  $\nu_\mu$  into the other two flavours, have been accounted for. The energy distribution of neutrino final states is therefore obtained from a modulated superposition of the three flavours, in the long-baseline approximation<sup>1</sup>, with coefficients taken from [1]. Neutrinos and antineutrinos are symmetrically produced in WIMP annihilations, and are detected indistinctly by current neutrino telescopes. This analysis is restricted to muon neutrino events at the detector, as will be described in Section 2.

## 2 Detector and Data Set

ANTARES is an underwater Cherenkov detector situated in the Mediterranean Sea 40 km offshore from Toulon. It is composed of 12 detection lines instrumented with photomultiplier tubes enclosed in optical modules [18]. ANTARES data analysis allows for energy and directional reconstruction of charged particle tracks originated from a neutrino interaction occurring around the detector. The very large background of muons produced in atmospheric interactions of cosmic rays is suppressed by considering events with arrival directions crossing the Earth. Under this condition, the Galactic Centre, located at a declination of  $-29.01^\circ$ , is visible from the detector latitude about 70% of the time [19].

---

<sup>1</sup>The  $E/L$  dependency of the oscillations are averaged out for GeV–TeV neutrino energies over the distance between the Earth and the Galactic Centre.

In this paper, 11 years of data collected with ANTARES between May 2007 and December 2017 are analysed, updating upon prior searches [20]. Signatures of neutrinos from DM annihilation are searched for in a data sample composed of reconstructed muon tracks originating from charged current (CC) interactions of neutrinos around the detector. A set of pre-selection cuts has been applied to discriminate these  $\nu_\mu$  CC-induced events from atmospheric muon background; this first discrimination is based on the zenith angle of provenience of the event and on the quality of the track reconstruction. Tracks are reconstructed in ANTARES from the position and times of photomultiplier hits, recorded in general from different detector lines. The quality parameter is, in the standard approach, a maximum likelihood  $\Lambda$  obtained with a multi-line reconstruction fit [21]. At low energies, however, it is possible to best reconstruct those tracks hitting only one line of the detector using a single-line reconstruction [22]; this fit is based on a  $\chi^2$  minimization and the  $\chi^2$  value serves as a quality parameter. The single-line reconstruction is more efficient for energies below  $\sim 100$  GeV.

The parameters  $\Lambda$  and  $\chi^2$  are used as quality indicator for multi-line and single-line tracks respectively. Additionally, an angular error estimate  $\beta$ , provided by the multi-line reconstruction fit, has been considered. Variable cuts have been applied as reported in Table 1, and the values yielding best sensitivity have been chosen to unblind the data, as explained later in section 3.1.

Fit	Cut value
Multi-line	$\Lambda > -5.2$
Multi-line	$\beta < 1^\circ$
Single-line	$\chi^2 < 0.7$
Both	$\cos \theta > 0$

Table 1: Final selection criteria applied to the data set. The quality of the multi-line reconstruction fit is evaluated by a likelihood  $\Lambda$  and angular error estimate  $\beta$ ;  $\chi^2$  characterises the single-line fit; the angle  $\theta$  is complementary to the zenith, such that  $\cos \theta > 0$  identifies an *upgoing* track, coming from across the Earth.

This sample is composed of 8976 tracks reconstructed with the multi-line algorithm and 2522 tracks with the single-line algorithm recorded over 3170 days of effective live-time; note that in the text that follows the term neutrinos stands for  $\nu + \bar{\nu}$ , as the events generated by their interactions are seen indistinguishably in current neutrino telescopes. Tracks are reconstructed with an angular resolution of the order of  $1^\circ$  at the energies relevant for this search [23]. Given its geometry and volume, the ANTARES telescope is optimised for the detection of neutrinos with energies from about 20 GeV to a few PeV. The DM analysis is, therefore, in the medium WIMP mass range. The amount of Cherenkov photons induced along the paths of the propagating charged particles is proportional to the amount of deposited energy and, consequently, the number of hit optical modules,  $N_{\text{HITS}}$ , is a good proxy of the neutrino energy  $E_\nu$ .

A set of simulated data has been produced in correspondence with the environmental and trigger conditions of each data run [24], and has been adapted to the specific DM

analysis through the use of weights reproducing the energy distribution  $dN_\nu/dE_\nu$  of each WIMP annihilation channel. The simulated data used for this search contain  $\nu_\mu$  CC induced muons; the contribution of muons from  $\nu_\tau \rightarrow \tau$  and subsequent  $\tau$  decay is not considered in the simulated sample used in this analysis.

The search is optimised on shuffled (*blind*) right-ascension data, which are unblinded after having established the best selection criteria. A newly released version of the ANTARES reconstruction software [21, 22] was run on the full data set. With the new processing and reconstruction of the data a considerable amount of livetime could be recovered with respect to the previous 9-year study [20].

The search method used for this analysis is the same as that used in the previous study [20], keeping into account the correction of a computation problem which affected the previous results [20].

### 3 Method

The signal from DM annihilation is expected to appear as a cluster of neutrino events scattered around the position of the Galactic Centre according to the  $J$ -factor profile, whose energy distribution reproduces the WIMP annihilation spectra [17]. This spatial cluster of signal events is to be found over a background of atmospheric neutrinos [25]. Both background estimation and search optimisation use shuffled (blinded) real data, by replacing the right ascension value with a random value between  $0^\circ$  and  $360^\circ$ . This random shuffle washes out any possible spatial clustering in correspondence to the source, permitting to use real data with fake coordinates to accurately describe the background distribution of events.

For identifying the signal, discriminating variables are the direction of the reconstructed neutrino track and the energy proxy,  $N_{\text{HITS}}$ , whose normalised distributions are used as an input in a likelihood function as probability density functions (PDFs). The signal PDF,  $\mathcal{S}$ , is built from simulated data weighted according to the WIMP annihilation spectra [17]; the background PDF,  $\mathcal{B}$ , is obtained from shuffled data. To assess the signal significance, a large number of skymaps (pseudo-experiments) are generated injecting an variable number of signal events,  $n_s$ , according to the signal PDF, over a set of  $N = n_s + n_{bg}$  events, with  $n_{bg}$  background events. The total number of events,  $N$ , is obtained from the total number of tracks in the data sample. The algorithm used to search for an excess of events coming from the region of the Galactic Centre is based on an unbinned likelihood function,  $\mathcal{L}$ , associated with each skymap (containing  $N$  events)

$$\begin{aligned} \log \mathcal{L}(n_s) = & \sum_{i=1}^N \log [n_s \mathcal{S}(\psi_i, N_{\text{HITS}}^i, q_i) \\ & + n_{bg} \mathcal{B}(\delta_i, N_{\text{HITS}}^i, q_i)] - n_{bg} - n_s, \end{aligned} \quad (5)$$

where  $\psi_i$  is the angular distance of the  $i$ -th event from the Galactic Centre;  $\delta_i$ , the Equatorial declination of the  $i$ -th event;  $N_{\text{HITS}}^i$ , the number of light hits recorded by the detector and associated with the  $i$ -th reconstructed track, and  $q_i$ , the quality of

the reconstruction. The likelihood maximisation returns the number of signal events,  $n_s^*$ , found to belong to a cluster around the fixed coordinates of the Galactic Centre  $(\alpha, \delta) = (266^\circ, -29.01^\circ)$ . The significance of a cluster is established by the test statistics, TS, which is a function of the ratio between the maximum and the pure background likelihood

$$TS = -\log \frac{\mathcal{L}(n_s^*)}{\mathcal{L}(n_s = 0)}. \quad (6)$$

To determine the significance of the observed TS, a series of pseudo-experiments is generated. This is performed by creating a large number of skymaps with a variable number of injected signal events,  $n_s$ , and running a maximum likelihood algorithm on each, returning the fitted number of events  $n_s^*$  for each of them. The number of events in each set of pseudo-experiments is subject to fluctuations following a Poisson distribution. To include this effect, a transformation through a Poisson function,  $\mathcal{P}$ , is performed, returning the TS as a function of the Poissonian mean  $\mu$ :

$$P(TS(\mu)) = \sum_{n_s^*=1}^N P(TS(n_s^*)) \mathcal{P}(n_s^*, \mu), \quad (7)$$

where  $P(TS)$  indicates the TS distribution.

The main source of systematic uncertainties comes from the determination of the neutrino track direction. The track reconstruction relies on the time resolution of the detector, dependent on the photomultiplier time spread, on the calibration and on possible space misalignment of the detector lines. The effect of systematic uncertainties was estimated in a previous analysis [23] to a total of 15%. A Gaussian smearing of 15% is applied to the signal PDFs to account for detector systematics.

### 3.1 Sensitivity of the search method

Following Neyman's prescription [26], an average upper limit on the number of signal events is computed from the median of the background test statistics  $\overline{TS}_0$ , compared with each distribution  $P(TS)$  for each pseudo-experiment set. The sensitivity is defined as the 90% C.L. upper limit for a measurement equal to the median of the background TS distribution. The analysis cuts are optimised to yield the best sensitivity (see Section 2 and values reported in Table 1). If, after unblinding, a value smaller than the median of the background TS is observed in the data, limits are set equal to the sensitivity .

In case of a non-observation, a limit of the total number of signal events in the data ( $\mu_{90}$ ) is converted into a limit on the integrated flux,  $\Phi_{\nu+\bar{\nu}}$ , through the acceptance,  $\mathcal{A}$ , and the livetime,  $t$ , as

$$\Phi_{\nu+\bar{\nu}} = \frac{\mu_{90}}{\mathcal{A} \cdot t}. \quad (8)$$

The acceptance is defined as the convolution of the effective area,  $A_{eff}$  [23], with each annihilation mode spectrum  $dN_\nu/dE_\nu$  [17]:

$$\mathcal{A}(M) = \int_{E_0}^M A_{eff}^\nu(E_\nu) \frac{dN_\nu(E_\nu)}{dE_\nu} dE_\nu + [\nu \rightarrow \bar{\nu}], \quad (9)$$



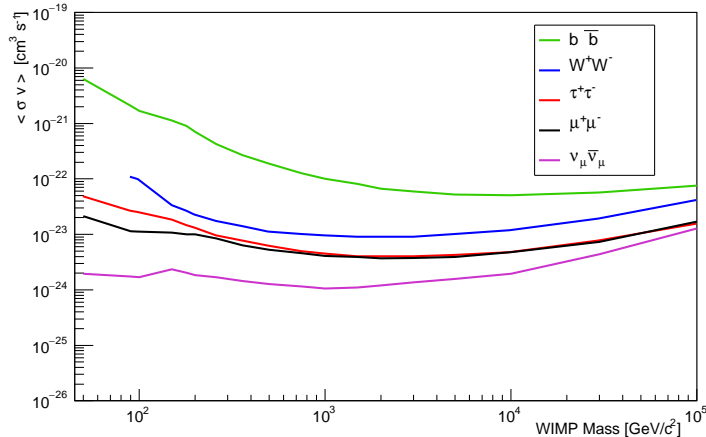


Figure 1: Upper limits at 90% C.L. on the thermally averaged cross section for WIMP pair annihilation as a function of the WIMP candidate mass set with 11 years of ANTARES data, shown for five independent annihilation channels (each with 100% branching ratio) and NFW halo model [11].

where  $M$  is the considered WIMP mass,  $E_0$  the energy threshold of the detector, determined from the first non-empty bin of the effective area, and  $[\nu \rightarrow \bar{\nu}]$  indicates a symmetric term for antineutrinos. The detector effective area increases with energy due to the raise with energy of the CC cross section, combined with the better track definition of high-energy events, and with an increase in the muon range, making such that partially contained tracks can still be measured. The acceptance calculation relies on spectra provided by PPC4. The integrated flux of Equation (8) is converted into a measurement (limit) on the thermally averaged cross section for WIMP annihilation  $\langle \sigma v \rangle$  using Equation (2), for a given  $J$ -factor assuming a specific parameterisation of the DM halo model.

## 4 Results

Upon unblinding, the TS computed for 11 years of ANTARES data is compatible with background. We observed a TS smaller than the background median for all cases (masses and channels), hence we set all limit values equal to the corresponding sensitivities. This measurement sets limits on the cross section for WIMP-pair annihilation shown in Figure 1 and computed according to Equation (2). This figure shows limits for the five most prominent WIMP pair annihilation channels:

$$\text{WIMP WIMP} \rightarrow b\bar{b}, \tau^+\tau^-, W^+W^-, \mu^+\mu^-, \nu\bar{\nu} \quad (10)$$

independently computed with 100% BR. The total amount of dark matter within a  $30^\circ$  angle around the Galactic Centre is taken into account, which corresponds to the

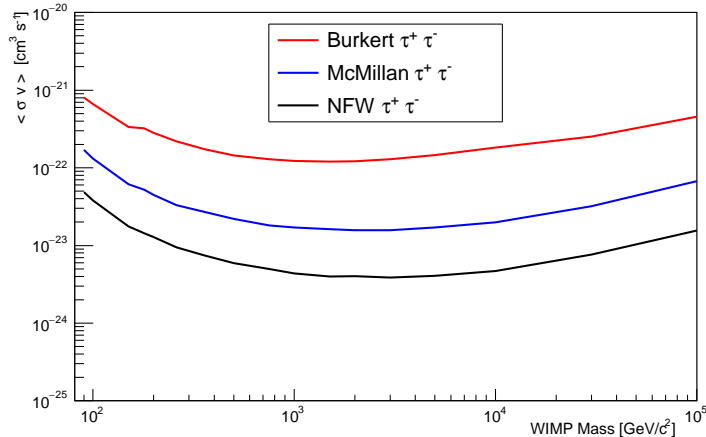


Figure 2: Upper limits at 90% C.L. on the thermally averaged cross section for WIMP pair annihilation as a function of the WIMP candidate mass set with 11 years of ANTARES data for three different halo models [11, 13, 14]. Here, only the  $\tau^+\tau^-$  channel is shown.

solid angle  $\Omega$  in Equation (1). Best limits are obtained for the direct  $\nu\bar{\nu}$  channel, as seen in Figure 1, which has the highest acceptance and the best sensitivity in number of events, due to the shape of the energy spectrum which peaks around the WIMP candidate mass; channels with steeply falling spectra such as  $b\bar{b}$  give the least stringent limits. Predictions on neutrino fluxes deriving from DM annihilation strongly rely on the parameterisation of the  $J$ -factor, as mentioned in Section 1.1. Figure 2 shows the 90% C.L. limits on  $\langle\sigma v\rangle$  for the  $\tau^+\tau^-$  channel for three different halo models. The NFW profile [11] gives predictions over one order of magnitude more stringent than *flat* profiles such as Burkert [14]. An intermediate result is achieved for the McMillan profile [13] which has an intermediate inner slope. The results presented in this work represent an improvement ranging from a factor 1.1 to 1.4 with respect to the previous 9-year study [20], according to the WIMP mass and channel considered.

## 5 Discussion and conclusions

Limits on the thermally averaged cross section  $\langle\sigma v\rangle$  for DM annihilation towards the Galactic Centre were placed using 11 years of ANTARES data. Some of the channels considered for this search also yield  $\gamma\gamma$  pairs as a final product. For this case, ANTARES limits are set in context with existing limits from  $\gamma$ -ray telescopes (Figure 3) for the  $\tau^+\tau^-$  channel. In particular, the HESS Galactic Centre survey [28] gives strong constraints thanks to the good visibility of this source from their location and to the prolonged observation campaign performed on this target. Note that both the MAGIC and the VERITAS detectors are located in the Northern Hemisphere and therefore they obtain

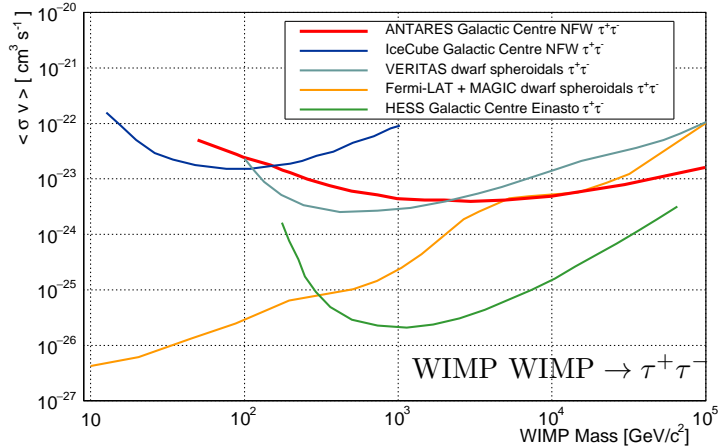


Figure 3: Limits on the thermally averaged cross section for WIMP pair-annihilation set with 11 years of ANTARES data, compared with current similar searches from IceCube [27] and from  $\gamma$ -ray telescopes HESS [28], VERITAS [29] and Fermi-LAT + MAGIC [30]. All curves are for the  $\tau^+\tau^-$  benchmark channel.

their limits on the WIMP pair annihilation cross section from a campaign of observation of dwarf spheroidal Galaxies [29, 30], not having the possibility to look directly into the Galactic Centre, if not with special settings for large zenith angle observations (e.g. [31]) with reduced sensitivity. Halo modeling in dwarf spheroidal Galaxies is subject to large uncertainties, and comparison with the Galactic Centre results is therefore not direct. The results shown for IceCube [27] are obtained with Deep Core data, a configuration where the whole IceCube detector acts as a veto for atmospheric muons. Because of the Galactic Centre visibility, this analysis is limited to WIMP masses up to 1 TeV/c<sup>2</sup>. All results shown in Figure 3 are obtained with the NFW profile, with the exception of the HESS result which refers to the Einasto DM halo model [32].

The current searches for dark matter performed with ANTARES will be continued with KM3NeT, which will instrument a total of about 1 km<sup>3</sup> of deep-sea water [33]. KM3NeT has a modular layout consisting of blocks of 115 detection lines each. Two modules are being deployed in a large volume (36 m inter-optical-modules and 90 m inter-line spacing) to form the ARCA high-energy detector, and one in a denser geometry instrumenting a smaller volume (9 m between optical modules and 20 m inter-line spacing) to form the ORCA low-energy detector. As the prescriptions for the WIMP candidate mass vary over a broad range of values, both ARCA and ORCA will contribute to DM searches.

## Acknowledgements

The authors acknowledge the financial support of the funding agencies: Centre National de la Recherche Scientifique (CNRS), Commissariat à l'énergie atomique et aux énergies

alternatives (CEA), Commission Européenne (FEDER fund and Marie Curie Program), Institut Universitaire de France (IUF), IdEx program and UnivEarthS Labex program at Sorbonne Paris Cité (ANR-10-LABX-0023 and ANR-11-IDEX-0005-02), Labex OCEVU (ANR-11-LABX-0060) and the A\*MIDEX project (ANR-11-IDEX-0001-02), Région Île-de-France (DIM-ACAV), Région Alsace (contrat CPER), Région Provence-Alpes-Côte d’Azur, Département du Var and Ville de La Seyne-sur-Mer, France; Bundesministerium für Bildung und Forschung (BMBF), Germany; Istituto Nazionale di Fisica Nucleare (INFN), Italy; Nederlandse organisatie voor Wetenschappelijk Onderzoek (NWO), the Netherlands; Council of the President of the Russian Federation for young scientists and leading scientific schools supporting grants, Russia; Executive Unit for Financing Higher Education, Research, Development and Innovation (UEFISCDI), Romania; Ministerio de Ciencia, Innovación, Investigación y Universidades (MCIU): Programa Estatal de Generación de Conocimiento (refs. PGC2018-096663-B-C41, -A-C42, -B-C43, -B-C44) (MCIU/FEDER), Severo Ochoa Centre of Excellence and MultiDark Consolidator (MCIU), Junta de Andalucía (ref. SOMM17/6104/UGR), Generalitat Valenciana: Grisolia (ref. GRISOLIA/2018/119), Spain; Ministry of Higher Education, Scientific Research and Professional Training, Morocco. We also acknowledge the technical support of Ifremer, AIM and Foselev Marine for the sea operation and the CC-IN2P3 for the computing facilities.

## References

- [1] M. Tanabashi and Particle Data Group. Review of particle physics. *Physical Review D*, 98(3):030001, Aug 2018.
- [2] N. W. Evans, J. L. Sanders, and Alex Geringer-Sameth. Simple j-factors and d-factors for indirect dark matter detection. *Phys. Rev. D*, 93:103512, May 2016.
- [3] G. Bertone. *Particle Dark Matter: Observations, Models and Searches*. Cambridge Univ. Press, Cambridge, 2010.
- [4] E. Tollet, A. V. Macciò, A. A. Dutton, G. S. Stinson, L. Wang, C. Penzo, T. A. Gutcke, T. Buck, X. Kang, C. Brook, A. Di Cintio, B. W. Keller, and J. Wadsley. NIHAO - IV: core creation and destruction in dark matter density profiles across cosmic time. *MNRAS*, 456(4):3542–3552, Mar 2016.
- [5] A. Pontzen and F. Governato. Cold dark matter heats up. *Nature*, 506(7487):171–178, Feb 2014.
- [6] P. Mollitor, E. Nezri, and R. Teyssier. Baryonic and dark matter distribution in cosmological simulations of spiral galaxies. *Mon. Not. Roy. Astron. Soc.*, 447(2):1353–1369, 2015.
- [7] G. R. Blumenthal, S. M. Faber, R. Flores, and J. R. Primack. Contraction of Dark Matter Galactic Halos Due to Baryonic Infall. *The Astrophysical Journal*, 301:27, Feb 1986.

- [8] A. Ghari, B. Famaey, C. Laporte, and H. Haggi. Dark matter-baryon scaling relations from Einasto halo fits to SPARC galaxy rotation curves. *AAP*, 623:A123, Mar 2019.
- [9] W. J. G. de Blok. The Core-Cusp Problem. *Advances in Astronomy*, 2010:789293, Jan 2010.
- [10] B. Famaey. Dark Matter in the Milky Way. *PoS*, FFP14:051, 2016.
- [11] J. F. Navarro, C. S. Frenk, and S. D. M. White. The Structure of cold dark matter halos. *Astrophys. J.*, 462:563, 1996.
- [12] F. Nesti and P. Salucci. The Dark Matter halo of the Milky Way, AD 2013. *Journal of Cosmology and Astroparticle Physics*, 2013(7):016, Jul 2013.
- [13] P. J. McMillan. The mass distribution and gravitational potential of the Milky Way. *MNRAS*, 2017.
- [14] A. Burkert. The Structure of Dark Matter Halos in Dwarf Galaxies. *Astrophys. J.*, 447(1):L25, 1995.
- [15] T. Sjöstrand, S. Mrenna, and P. Skands. PYTHIA 6.4 physics and manual. *Journal of High Energy Physics*, 2006(5):026, May 2006.
- [16] G. Corcella, I. G. Knowles, G. Marchesini, S. Moretti, K. Odagiri, P. Richardson, M. H. Seymour, and B. R. Webber. HERWIG 6: an event generator for hadron emission reactions with interfering gluons (including supersymmetric processes). *Journal of High Energy Physics*, 2001(1):010, Jan 2001.
- [17] M. Cirelli, G. Corcella, A. Hektor, G. Hutsi, M. Kadastik, P. Panci, M. Raidal, F. Sala, and A. Strumia. PPC 4 DM ID: A Poor Particle Physicist Cookbook for Dark Matter Indirect Detection. *JCAP*, 1103:051, 2011. [Erratum: *JCAP*1210,E01(2012)].
- [18] Ageron, M. et al. ANTARES: The first undersea neutrino telescope. *Nuclear Instruments and Methods in Physics Research A*, 656(1):11–38, Nov 2011.
- [19] T. Pradier. Coincidences between gravitational wave interferometers and high energy neutrino telescopes. *Nuclear Instruments and Methods in Physics Research Section A: Accelerators, Spectrometers, Detectors and Associated Equipment*, 602(1):268 – 274, 2009.
- [20] A. Albert et al. Results from the search for dark matter in the Milky Way with 9 years of data of the ANTARES neutrino telescope. *Phys. Lett. B*, 769:249, 2017. [Erratum: *Phys. Lett.B*(2019)].
- [21] S. Adrián-Martínez et al. Search for cosmic neutrino point sources with four years of data from the antares telescope. *The Astrophysical Journal*, 760(1):53, nov 2012.

- [22] J. A. Aguilar et al. A fast algorithm for muon track reconstruction and its application to the antares neutrino telescope. *Astroparticle Physics*, 34(9):652 – 662, 2011.
- [23] A. Albert et al. First all-flavor neutrino pointlike source search with the ANTARES neutrino telescope. *Phys. Rev. D*, 96(8):082001, Oct 2017.
- [24] A. Margiotta. Common simulation tools for large volume neutrino detectors. *Nuclear Instruments and Methods in Physics Research A*, 725:98–101, Oct 2013.
- [25] M. Honda, T. Kajita, K. Kasahara, S. Midorikawa, and T. Sanuki. Calculation of atmospheric neutrino flux using the interaction model calibrated with atmospheric muon data. *Phys. Rev. D*, 75(4):043006, Feb 2007.
- [26] J. Neyman. Outline of a Theory of Statistical Estimation Based on the Classical Theory of Probability. *Philosophical Transactions of the Royal Society of London Series A*, 236(767):333–380, Aug 1937.
- [27] M. G. Aartsen et al. Search for Neutrinos from Dark Matter Self-Annihilations in the center of the Milky Way with 3 years of IceCube/DeepCore. *Eur. Phys. J. C*, 77:627, 2017.
- [28] H. Abdallah, A. Abramowski, F. Aharonian, F. Ait Benkhali, A. G. Akhperjanian, E. Angüner, M. Arrieta, P. Aubert, M. Backes, and A. Balzer. Search for Dark Matter Annihilations towards the Inner Galactic Halo from 10 Years of Observations with H.E.S.S. *Phys. Rev. Lett.*, 2016.
- [29] S. Archambault et al. Dark Matter Constraints from a Joint Analysis of Dwarf Spheroidal Galaxy Observations with VERITAS. *Phys. Rev. D*, 95:082001, 2017.
- [30] M. L. Ahnen et al. Limits to dark matter annihilation cross-section from a combined analysis of MAGIC and Fermi-LAT observations of dwarf satellite galaxies. *Journal of Cosmology and Astroparticle Physics*, 2016(2):039, Feb 2016.
- [31] J Albert et al. Observation of Gamma Rays from the Galactic Center with the MAGIC Telescope. *The Astrophysical Journal*, 638(2):L101–L104, Feb 2006.
- [32] J. Einasto. On the Construction of a Composite Model for the Galaxy and on the Determination of the System of Galactic Parameters. *Trudy Astrofizicheskogo Instituta Alma-Ata*, 5:87–100, Jan 1965.
- [33] S. Adrián-Martínez et al. Letter of intent for KM3NeT 2.0. *Journal of Physics G Nuclear Physics*, 43(8):084001, Aug 2016.